Remote Sensing of Environment 199 (2017) 360–369

Contents lists available at ScienceDirect

Remote Sensing of Environment

journal homepage: www.elsevier.com/locate/rse

High spatial resolution spectral unmixing for mapping ash species across a complex urban environment

Jennifer Pontius[a,*], Ryan P. Hanavan[b], Richard A. Hallett[c], Bruce D. Cook[d], Lawrence A. Corp[e]

[a] University of Vermont Rubenstein School of Environment and Natural Resources, USDA Forest Service Northern Research Station, 81 Carrigan Drive, Burlington, VT 05405, United States
[b] US Forest Service, Northeastern Area State and Private Forestry, United States
[c] US Forest Service, Northern Research Station, United States
[d] NASA, Goddard Space Flight Center, United States
[e] NASA, Biospheric Science Branch, United States

ARTICLE INFO

Keywords:
Hyperspectral
Emerald ash borer
OBIA
Forest species classification
GLiHT
Spectral unmixing
Forest decline
Forest health

ABSTRACT

Ash (*Fraxinus* L.) species are currently threatened by the emerald ash borer (EAB; *Agrilus planipennis* Fairmaire) across a growing area in the eastern US. Accurate mapping of ash species is required to monitor the host resource, predict EAB spread and better understand the short- and long-term effects of EAB on the ash resource. Hyperspectral remote sensing technologies have been used to successfully map forest species, although most efforts are focused on healthy canopies for relatively homogeneous forested stands. This study uses imagery collected by the NASA Goddard LiDAR, Hyperspectral and Thermal (GLiHT) airborne imager to map ash species at the tree level in an EAB infested urban setting. The overall goal of the study is to understand how canopy condition impacts species mapping accuracy and identify data collection and image processing techniques to more accurately map the location of ash species in infested regions.

Results indicate that while overall independent validation mapping accuracy of ash and non-ash trees was 81%, correct identification of ash canopies dropped from 62% for vigor 1 trees to 22% for vigor 2 trees. To minimize these errors, we developed a multiple endmember, spectral unmixing technique to overcome challenges presented by a spectrally complicated target in a complex urban environment. This hinges on the use of endmember spectra from trees across a range of canopy condition, including the derivation of vegetation indices to inform the spectral unmixing calibration. This approach was more accurate than calibrations performed using traditional unmixing based only on pure endmember spectra.

Implications for this work suggest that urban forest managers may attain more accurate maps by conducting remote sensing data collections prior to infestation while the trees are still healthy. Where this is not possible, mapping efforts must reflect a range of canopy conditions and include vegetation indices concurrent with reflectance data. The resulting ash species maps provide urban forest managers spatially explicit products to help estimate the extent of possible impacts in their communities, guide the implementation of management and monitoring efforts and provide the basis for planning as EAB continues to spread.

1. Introduction

Biological invasions of non-native insects are both a threat to biodiversity and ecosystem stability (Pimentel et al., 2001; Simberloff, 2000). Approximately 360 non-native insects were established in United States by the mid 1990's (Liebhold et al., 1995), reaching 455 by 2011 (Aukema et al., 2011). Phloem feeding and wood boring insects are the most costly feeding guild resulting in approximately $1.7 billion per year in local government expense and another $830 million in lost property value (Aukema et al., 2011). Intercepting these invaders before or during arrival is optimal. However, once arrival and establishment is achieved, early detection becomes critical in reducing the impact of spread.

The emerald ash borer, *Agrilus planipennis* Fairmaire (EAB), is an exotic phloem feeding woodborer (Coleoptera: Buprestidae) introduced from Asia, and has become one of the most devastating insects to successfully establish and spread in North America (Klooster et al., 2014). Widespread ash, *Fraxinus* spp., mortality was reported in Southeastern Michigan, USA, and Essex Co, Ontario, Canada in 2002 (Haack et al., 2002) and has been confirmed in 30 American states, and Canadian

* Corresponding author.
E-mail address: Jennifer.pontius@uvm.edu (J. Pontius).

http://dx.doi.org/10.1016/j.rse.2017.07.027
Received 9 December 2016; Received in revised form 20 June 2017; Accepted 21 July 2017

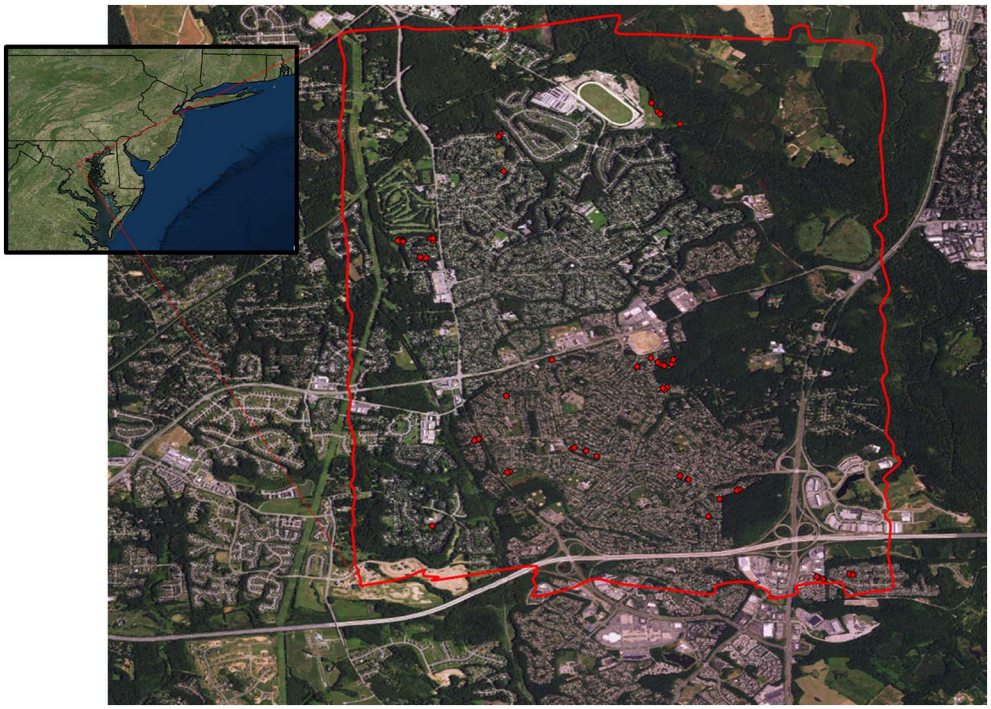

Fig. 1. Extent of the Bowie GLiHT imagery collection with ash calibration canopies in red. (For interpretation of the references to color in this figure legend, the reader is referred to the web version of this article.)

Provinces, Ontario and Quebec (www.emeraldashborer.info). Adult EABs emerge in late spring and adult females lay eggs under the bark (Bauer et al., 2004). Larval feeding scores the outer sapwood and disrupts water transport in vascular tissue (Cappaert et al., 2005). Damage increases with increasing EAB density causing decline and eventual tree mortality (McCullough et al., 2009).

Management costs (treatment, removal and replacement of ash trees) could reach $10.7 billion just for trees on developed land in communities in the eastern US (Kovacs et al., 2010) and an additional $13–26 billion in the Midwestern US (Sydnor et al., 2007) by 2019. Given the severe economic impact of EAB to our urban areas in particular, accurate mapping of existing ash distribution and condition is critical to help manage the economic impact of further establishment and spread of this invasive insect.

Remote sensing data has been successfully used to map, not only broad vegetation types (NLCD, USGS) but also the distribution of individual tree species (e.g., Martin et al., 1998; Ustin and Xiao, 2001; Pontius et al., 2005a; Plourde et al., 2007). These efforts are usually based on healthy and homogeneous forested stands. More recently, Murfitt et al. (2016) mapped ash canopies in contiguous forest stands in southeastern Ontario using high spatial resolution WorldView-2 imagery. They classified ash trees with 60–63% accuracy using a multiband watershed level segmentation algorithm and random forest classifier. Zhang et al. (2014) used high spatial resolution aerial imagery, commercial ground and airborne hyper-spectral data to map ash canopies in Ontario with 63% accuracy.

Urban species mapping presents additional complications due to the influence of understory and groundcover on the spectral signatures of small, open grown trees. In locations where EAB has caused widespread decline and mortality, spectral identification of ash species becomes even more complicated due to changes in foliar chemistry and canopy structure in declining trees. None of these efforts explored how species mapping accuracy changes across a range of canopy condition or how to improve accuracy by modifying classifications to account for trees in various stages of decline.

Because different tree species often have similar spectral characteristics, even subtle changes in reflectance resulting from different canopy conditions can lead to classification error. Such spectral confusion is common in declining stands, where stress symptoms alter foliar chemistry and canopy structure, resulting in uncharacteristic spectral signatures for the target species. This is particularly problematic for ash, which is spectrally similar to many of its co-occurring species (Souci et al., 2009). In addition to classification error introduced by canopies in various stages of decline, mapping species in urban areas is confounded by the spatial heterogeneity and spectral diversity found in developed environments. Canopies may be underlain by either pavement, cement, dirt, grass or various mixes of ground cover that influence the spectral signal, particularly for declining, sparse trees.

To apply remote sensing technology to urban areas successfully, especially in the face of declining forest health, sensors and image processing techniques need to be developed that will overcome challenges presented by the urban environment. One promising image processing technique called spectral unmixing (Keshava and Mustard, 2002) has the potential to help overcome issues caused by fine scale spectral heterogeneity and mixed pixel effects characteristic of urban environments. Spectral unmixing has been effective for detecting tree species and other vegetation abundances using spatial resolutions ranging from 17 m to 30 m (e.g., Small, 2001; Pontius et al., 2005a; Plourde et al., 2007). However, successful spectral unmixing of fine spatial resolution data (i.e., 1–3 m), has been largely limited to non-forested areas (e.g., Miao et al., 2006).

This study uses imagery collected by the NASA Goddard LiDAR, Hyperspectral and Thermal (GLiHT) airborne imager (Cook et al., 2013) to map ash species at the tree level in an EAB infested, urban setting. The combination of hyperspectral data combined with high spatial resolution presents a “best case” approach to mapping a declining species in a challenging urban setting. The overall goal of the study is to understand how canopy condition impacts species mapping accuracy and identify data collection and image processing techniques that minimize these errors in EAB infested regions.

Table 1
Common broad and narrow-band vegetation indices stacked with hyperspectral wavelengths for the minimum noise fraction transform. Indices with asterisk are available using ENVI's vegetation index tool.

Acronym	Vegetation index	Citation
Aoki	Aoki Stress	Aoki et al., 1981
ARI1*	Anthocyanin Reflectance Index 1	Gitelson et al., 2001
ARI2*	Anthocyanin Reflectance Index 2	Gitelson et al., 2001
CF	Chlorophyll fluorescence	Mohammed et al., 1995
CI	Curvature Index	Zarco-Tejada et al., 2002
CRI1*	Carotenoid Reflectance Index 1	Gitelson et al., 2003
CRI2*	Carotenoid Reflectance Index 2	Gitelson et al., 2003
CS1	Carter Stress 1	Carter, 1994
CS2	Carter Stress 2	Carter, 1994
Datt 1	Datt Stress 1	Datt, 1998
Datt 2	Datt Stress 2	Datt, 1999
DCI	Derivative Chlorophyll Index	Zarco-Tejada et al., 2002
DVI	Difference Vegetation Index	Tucker, 1979
EZ	Elvide and Zhikang Stress	Elvidge and Chen, 1995
FP	Filella and Penuelas Stress	Filella and Penuelas, 1994
GI	Greeness Index	Smith et al., 1995
GM	Gitelson and Merzlyac Stress 1	Gitelson and Merzlyak, 1994
GMb	Gitelson and Merzlyac Stress 2	Gitelson and Merzlyak, 1994
Mac	Maccioni Stress	Maccioni et al., 2001
MCARI	Modified Chlorophyll Absorption Ratio Index	Daughtry et al., 2000
MCARI2	Modified Chlorophyll Absorption Ratio Index Improved	Haboudane et al., 2004
MRE NDVI	Modified Red Edge Normalized Difference Vegetation Index	Sims and Gamon, 2002
MRESR*	Modified Red Edge Simple Ratio	Sims and Gamon, 2002
MSR*	Modified Simple Ratio	
MTVI	Modified Triangular Vegetation Index	Haboudane et al., 2004
MTVI2	Modified Triangular Vegetation Index - Improved	Haboudane et al., 2004
NDVI*	Normalized Difference Vegetation Index	Rouse et al., 1973
NPCI	Normalized Pigment Chlorophyll Index	Penuelas et al., 1994
NPQI	Normalized Phaeophytinization Index	Barnes, 1992
OSAVI	Optimized Soil Adjusted Vegetation Index	Rondeaux et al., 1996
PRI*	Photochemical Reflectance Index	Gamon et al., 1990, 1997; Rahman et al., 2001
PSND1	Pigment Specific Normalized Difference 1	Blackburn, 1998
PSSR2	Pigment Specific Normalized Difference 2	Blackburn, 1998
PSRI*	Plant Senescence Reflectance Index	Merzlyak et al., 1999
RDVI	Renormalized Difference Vegetation Index	Roujean and Breon, 1995
RENDVI*	Red Edge Normalized Difference Vegetation Index	Gitelson and Merzlyak, 1994
REIP*	Red Edge Inflection Point	Baret et al., 1992
RGRI*	Red Green Ratio Index	Gamon and Surfus, 1999
RVI	Ratio Vegetation Index	Pearson and Miller, 1972
SIPI*	Structure Insensitive Pigment Index	Penuelas et al., 1995
SRPI	Simple Ratio Pigment Index	Penuelas et al., 1993
TVI	Triangular Vegetation Index	Broge and Leblanc, 2001
VOG*	Vogelmann Stress	Vogelmann et al., 1993
VREI1*	Vogelmann Red Edge Index 1	Vogelmann et al., 1993

2. Methods

2.1. Study area

Imagery and ground reference data were collected for the city of Bowie, Maryland, USA in June of 2012 (Fig. 1). This temperate region, along the eastern US coast, is typically dominated by oak-hickory-pine forests. But urban and suburban regions such as Bowie are highly landscaped with a mix of ornamentals and native species. At the time of this study, the city itself was responsible for almost 9000 street trees. Of these, Bowie reported over 800 city owned ash trees that were in varying stages of decline due to the presence of EAB. The city has small patches of dense mixed forests, but is predominantly composed of sparsely forested suburban areas dominated by impervious surfaces. The first detection of EAB in Maryland was on August 28, 2003, only one year later than the first detection in the United States (www.emeraldashborer.info). Infested nursery stock was the likely culprit and initial eradication efforts were unsuccessful. In Bowie EAB was confirmed June 14, 2011 (Maryland Department of Agriculture, http://mda.maryland.gov/plants-pests/Pages/eab-current.aspx).

Urban areas like Bowie are highly susceptible to forest pest introduction and establishment because of their proximity to trade and international commerce centers. Trees planted in urban forests may also be imported nursery stock, another source for accidental introduction (Niemelä and Mattson, 1996). There are also similarities in host families and genera between North America, Europe and Asia that facilitate establishment potential (Niemelä and Mattson, 1996).

2.2. Ground reference data

Ground reference data for image calibration were collected within one week of image data acquisition. Trees were selected for image calibration to ensure that a range of ash vigor and understory composition were captured, along with a broad spatial distribution across the study area (Fig. 1). Additional criteria for calibration tree selection included: canopy dominant or co-dominant status with crowns that were at least 2 m^2. Selected trees were geo-located using a Trimble® GPS for direct comparison to corresponding pixels within the imagery. Data collected for each tree included: species; DBH; crown position (i.e., dominant, co-dominant, or sub-canopy); and a suite of decline symptoms common to EAB infestation (Pontius et al., 2008, Pontius and Hallett, 2014). We used methods described by Cooke et al. (1996) to assign each tree to a vigor class designed to capture the overall condition of the canopy (where Vigor 1 = healthy, Vigor 5 = dead). This metric is based on the percent of the canopy impacted by branch mortality, twig dieback, foliage discoloration or dwarfed leaves. Because EAB shows no preference for the various ash species, species mapping was performed at the genus level only—i.e., all *Fraxinus* species were agglomerated for mapping.

The resulting calibration data set included 53 ash canopies representing a range of ash condition (twenty-two vigor 1, eleven vigor 2, ten vigor 3 and ten vigor 4 canopies). Of these, a high-quality subset, including only canopy dominant trees with crowns > 1 m diameter that were clearly identifiable in the imagery, was created for end-member collection to minimize georegistration error or mixing with adjacent canopies. The resulting subset of 37 canopies for classification calibration included: thirteen vigor 1, nine vigor 2, seven vigor 3 and eight vigor 4 canopies. Dead trees were not included in calibration or validation data sets.

2.3. Image data

In June 2012, The GLiHT sensor (http://gliht.gsfc.nasa.gov/about/) mounted on a fixed wing aircraft collected 1 m resolution data over the target area covering approximately 4800 ha. Input imagery was geometrically corrected in house with a resulting accuracy of ~10 cm (1 σ), Cook et al., 2013) with no additional corrections required to match field GPS locations to image canopies. Radiometrically calibrated reflectance data included 114 unique bands covering a spectral range of approximately 400 nm to 1000 nm with 5 nm spectral resolution. In addition, 41 common vegetation indices (Table 1) were calculated in ENVI (v. 5.3) using ENVI's automated band math functions. These indices were selected based on their documented importance in ash condition mapping (Pontius et al., 2008; Pontius, 2014), or availability of automated calculation algorithms in tools such as ENVI. Stacked together, this resulted in a 155 band image for spectral unmixing

algorithms.

2.4. Ash species classification

Spectral mixture analysis (Boardman and Kruse, 2011; Plaza et al., 2009) is a technique used for vegetation mapping which determines sub-pixel fractional abundance of target endmembers (Roberts et al., 1998; Elmore et al., 2000; Small, 2001; Williams and Hunt, 2002; Miao et al., 2006). This approach is particularly useful for coarse spatial resolution imagery where spectra for a given pixel are characterized by a mix of constituents on the ground. We used a mixture-tuned matched filtering (MTMF) spectral unmixing algorithm, which differs from traditional spectral mixture analysis in that it is based on spectrally "pure" endmembers for only the target of interest, producing both likelihood an infeasibility scores for endmember presence in each pixel (e.g. Plourde et al., 2007; Pontius et al., 2005a).

In urban areas, high spatial resolution remote sensing data is required due to the spatial heterogeneity characterized by a mix of tree canopy vegetation, woody materials and the understory beneath (lawn, sidewalk, road, shrubs). This is particularly true for EAB infested ash with noticeably thinning canopies. Given this complicated spectral environment we chose to explore the usefulness of spectral unmixing techniques to map ash canopies.

We set out to compare the use of MTMF-based spectral unmixing based on either the hyperspectral reflectance only (HS) or the hyperspectral reflectance with the addition of a suite of vegetation indices (HS-VI). In addition, we compared the accuracy resulting from various endmember collection approaches. This included aggregating endmember spectra as: 1) all ash canopies regardless of health (All Vigor), 2) vigor 1 ash canopies only (Vigor 1), and 3) separate endmembers for each of the four vigor class polygons (Unique Vigor). This included 13, 9, 7 and 8 canopies for Vigor Classes 1–4 respectively. This combination of two input imagery choices and three endmember collection techniques resulted in 6 possible results to compare to determine the best approach for classifying ash canopies.

2.5. MTMF-based spectral unmixing

Our Mixture-tuned match filtering (MTMF)-based spectral unmixing begins with a minimum noise fraction (MNF) transform to maximize signal:noise and reduce autocorrelation among input bands prior to unmixing. Similar to a principal components transform, MNF (Green et al., 1998; Boardman and Kruse, 2011) reduces the dimensionality of hyperspectral reflectance data by reprojecting the data onto orthogonal vectors that account for decreasing amounts of spectral variability in the imagery. MNF includes an additional step that segregates noise from data. The outcome is a new n-dimensional image, where the first few bands include the most information and the latter bands include progressively more noise.

The MNF transform was conducted on both the hyperspectral imagery (HS) alone, and the hyperspectral imagery with vegetation indices stacked (HS-VI) to determine if the inclusion of vegetation condition specific indices improved classification. The ideal number of MNF bands can typically be assessed using the spatial coherence threshold plot and including only those bands that maintain a spatial coherence greater than zero. Because spatial coherence decreases logarithmically across MNF bands, we tested a range of MNF band numbers near that zero threshold and determined that the first 25 bands from the MNF transforms were ideal for capturing the full signal in both the hyperspectral and hyperspectral plus vegetation indices images. Therefore, full unmixing and accuracy assessments for all 6 possible approaches were limited to these 25 bands for subsequent classification steps.

Endmember spectra from the 37 calibration trees were extracted from hand digitized canopy polygons (e.g. Fig. 2) to ensure that pixels from the full canopy, minus any edge or gap pixels, were included for calibration. This minimized registration errors and errors introduced by mixed pixels.

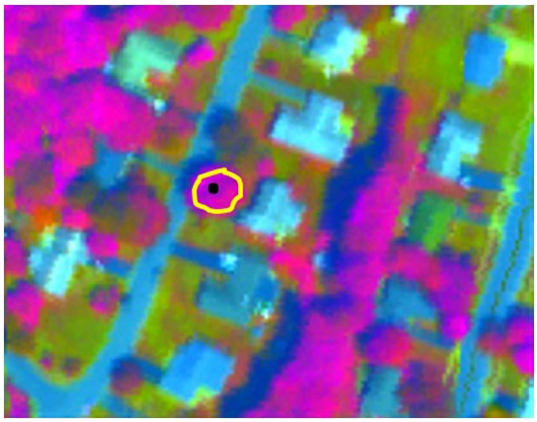

Fig. 2. Sample endmember canopy digitization (yellow) to capture full variability in the target ash canopy (GPS point in black) while eliminating mixed-canopy, edge pixels. (For interpretation of the references to color in this figure legend, the reader is referred to the web version of this article.)

Once endmembers were identified in each image, MTMF was performed on the 25 band MNF outputs in ENVI (v. 5.0) image processing software. Mixture-tuned matched filtering (Boardman and Kruse, 2011) detects abundances of user-defined endmembers by "unmixing" the pixels from "background" material. MTMF maximizes the response of the endmember in the MNF image and suppresses the background, thus "matching" the known signature. Because the background—e.g., anything other than ash—is suppressed, it is not necessary to identify endmembers of other non-interest targets. This process produces an image where each pixel is assigned a matched filter (MF) score and an infeasibility (INF) score for each represented endmember. The matched filter score represents how well the pixel spectra match the endmember (e.g., a value between 0 and 1.00, where 1.00 represents a perfect match with the endmember). The accompanying infeasibility score can be used to quantify the likelihood of false positives. Optimum MTMF results to identify the species of interest are pixels with high matched filter scores and low infeasibility scores.

Rather than use simple MF and INF thresholds to map ash, we used logistic regression based on the full set of available ash calibration canopies (53 tree canopies described above) to create a probability function for ash based on input INF and MF values. This model provided probability coefficients to apply to the MTMF imagery on a pixel by pixel basis resulting in a raster with values from 0 to 1 representing the probability that a given pixel contains ash. This logistic model was repeated for each of the 6 possible imagery/endmember calibration approaches.

2.6. Imagery segmentation

The high spatial resolution of the GLiHT imagery combined with the highly variable nature of tree canopies with complex geometries and differential illumination makes a pixel-based approach to tree canopy delineation impractical. Instead, we used Definiens Developer (v. 7) to segment the pixel-based raster to an object-based shapefile using a multiresolution segmentation to differentiate forest/non-forest and a watershed segmentation to delineate tree crowns within the forest class. Segmentation is based on spectral homogeneity metrics in combination with spatial and geometric parameters (size, shape, texture, etc.) to best capture objects that realistically depict individual trees. Several segmentation algorithms are commonly available (e.g. Yang et al., 2014a, b), with segmentation parameters that vary by application. This requires comparisons of various approaches to identify values that produce objects of the appropriate size and shape (Yang et al., 2015). We used an iterative exploration of various spectral and shape weightings,

Fig. 3. Close up of true color imagery (top) and segmented tree canopies based on NDVI thresholds for canopy delineation and R,G,B and NIR bands for canopy segmentation.

informed by previous literature, our knowledge of the typical canopy size, shape, reflectance characteristics and spatial context, imagery resolution, and characteristics of the landscape to identify spectral weights and segmentation settings to best capture individual tree canopies in this complex urban environment. We found that using blue, green, red and NIR (weighted × 2) bands, with a scale parameter (35), Shape = 0.7, Compactness = 0.9, Scale Parameter = 35, ensured that tree canopies were consistently differentiated from non-forest objects (Fig. 3). For all segmented objects, mean ash probability values from the logistic model (described above) were used to classify all canopies with an ash probability > 0.5 as ash and < 0.5 as non-ash canopies.

2.7. Accuracy assessment

To assess the accuracy of the resulting ash maps, we used an independent field inventory of street trees compiled by the city of Bowie, Maryland for their Urban Greening Report (http://www.cityofbowie.org/DocumentCenter/View/25). Main stems for street trees in the Bowie tree inventory were identified by species and geolocated in the field using a Trimble® GPS. From the over 8000 mapped trees across the city a random subset of 290 tree canopies were selected representing the ten most common species in Bowie, including 76 white or green ash (Table 2, Fig. 4). Polygons for lawns/field and impervious surfaces were also included to verify accuracy in distinguishing sick ash from the common understory beneath them.

Contingency tables were created from these data that quantify user's accuracy (the percentage of ash classified in the image pixels that were truly ash) and producer's accuracy (the percentage of field ash canopies correctly identified in the image; Congalton, 2001) as well as overall map accuracy. In addition, accuracy for each of the 37 ash calibration polygons was examined by field assigned vigor class to determine if accuracy degraded with increasing ash decline symptoms.

Table 2
Independent validation species counts.

Common name	Scientific name	Inventory count	Validation count
Silver maple	*Acer saccharinum*	628	23
Maple (other)	*Acer* sp.	2645	22
Ash species	*Fraxinus* sp.	379	76
Honey locust	*Gleditsia triacanthos*	954	27
American sycamore	*Platanus occidentalis*	860	29
Callery pear	*Pyrus calleryana*	459	26
Oak species	*Quercus* sp.	211	55
Field/lawn	*x*		18
Impervious surfaces	*x*		14

3. Results and discussion

The side by side comparison of the six calibration approaches (HS vs. HS-VI imagery and All Vigor, Vigor 1 or Unique Vigor endmembers) allowed us to identify the most accurate approach for mapping ash species when there is a broad range of ash condition in the target mapping area.

3.1. Comparison of HS vs. HS-VI imagery

Across all three endmember configurations, the hyperspectral plus vegetation imagery (HS-VI) resulted in marginally better logistic model fits (Table 3), and significantly higher ash identification accuracy than the hyperspectral imagery alone ($t_{(37.62)} = 3.55$, $p = 0.0005$). Because the number of input MNF bands was constant across these calibration approaches, these results indicate that the inclusion of vegetation indices is not simply an overfit, but instead provides information relevant to species mapping that is not captured in the reflectance itself.

It is uncommon for hyperspectral classification efforts to include vegetation indices in addition to the reflectance data. However, vegetation indices have been widely used in ecological assessments (Kerr and Ostrovsky, 2003). The most common is the Normalized Difference Vegetation Index (NDVI), which is strongly correlated with both physiological and structural vegetation characteristics including: aboveground net primary productivity, absorbed photosynthetically active radiation, and leaf area index (Cihlar et al., 1991). Vegetation indices have also been used for coarser assessments of land cover type mapping (Homer et al., 2015), vegetation density and biodiversity assessments (Broge and Leblanc, 2001; Peddle et al., 2001; Waring et al., 2006a, b) and forest type mapping (de Melo Figueiredo et al., 2015; Dymond et al., 2002).

These results show that the addition of vegetation indices captures information that may help discriminate among tree species (Fig. 5). Indices that target specific structural characteristics such as leaf area index or vegetation density, vary from species to species. For example, red maple tends to form full dense canopies in open grown habitats common to urban settings. In contrast, open-grown ash commonly remain single stemmed and fine branched (with a larger component of impervious surface or understory vegetation apparent in the canopy spectra). Incorporating indices specifically designed to capture these structural differences improves our ability to distinguish ash from other species.

This is exemplified in our imagery where we found significant differences among species for many of the vegetation indices included in our analysis. For example, ash species had significantly lower NDVI values compared to all other common species ($p < 0.0001$) (Fig. 5). In contrast, the Photochemical Reflectance Index (PRI) for ash was higher than all other species, but was only significantly able to distinguish ash from sycamore ($p < 0.0001$). However, different vegetation indices could distinguish different sets of species, indicating that there is no one set of “ideal” indices to include in species classifications.

These results indicate that using a combination of vegetation indices

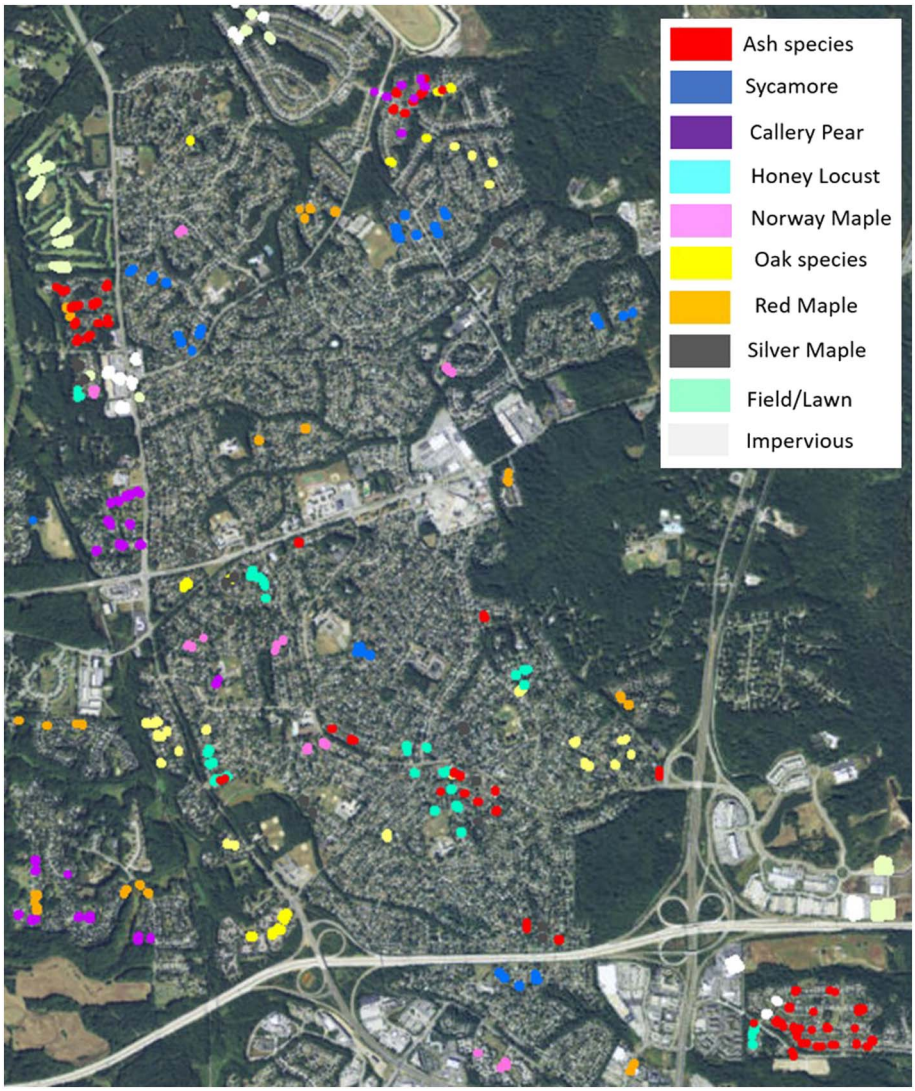

Fig. 4. Independent validation polygons selected randomly from the Bowie street tree inventory.

Table 3
Ash calibration logistic model fit for the six imagery and endmember combinations considered. All values range from 0 to 1.

Imagery combination	Endmember configuration	Logistic misclassification rate	Overall accuracy	Ash identification accuracy
HS_VI	Unique endmembers by vigor class	0.18	0.81	0.46
HS_VI	Vigor 1 ash	0.21	0.78	0.30
HS_VI	All ash	0.26	0.74	0.11
HS	Unique endmembers by vigor class	0.21	0.79	0.08
HS	Vigor 1 ash	0.22	0.78	0.03
HS	All ash	0.22	0.78	0.00

and hyperspectral data as input to the minimum noise fraction transform improves our ability to distinguish ash from other common tree species in a region of mixed forest health.

3.2. Comparison of endmember configurations

Traditionally, endmembers used for spectral unmixing are selected to represent "pure reflectance" of the target object. These spectra can be derived from cataloged spectral files or known target objects within the image. Pixel based endmembers are further refined using the pixel purity index (PPI) to limit endmembers to the most spectrally pure pixels. These endmembers represent idealized examples of the spectral signature for the given target. For classifying tree species this typically involves collecting endmember spectra from dense, healthy canopies with minimal mixing from other tree species, understory or surface materials. This approach works well when there is consistency in the spectral signature of target objects throughout the image.

Given that spectral unmixing results are highly dependent on the input endmembers, we tested to see if this traditional approach would work in a region of highly variable crown condition for ash species. Endmember configurations included using only dense, vigor 1 canopies (traditional approach) and two options to capture the full range of ash condition: creating an endmember group that included ash canopy pixels across all four vigor classes (All Vigor), and creating separate endmember groups for each ash vigor class (Unique Vigor).

Comparing all three endmember configurations using accuracy statistics from both HS and HSVI imagery inputs we found that using Unique Vigor endmembers was significantly more accurate than using only Vigor 1 endmembers or aggregated endmembers across all vigor classes. This was true in both identifying ash ($p = 0.014$, 37% mean producers accuracy) and distinguishing ash from other species (81% mean overall accuracy $p = 0.008$) (Table 3). There was no significant difference between using only Vigor 1 and aggregated All Vigor

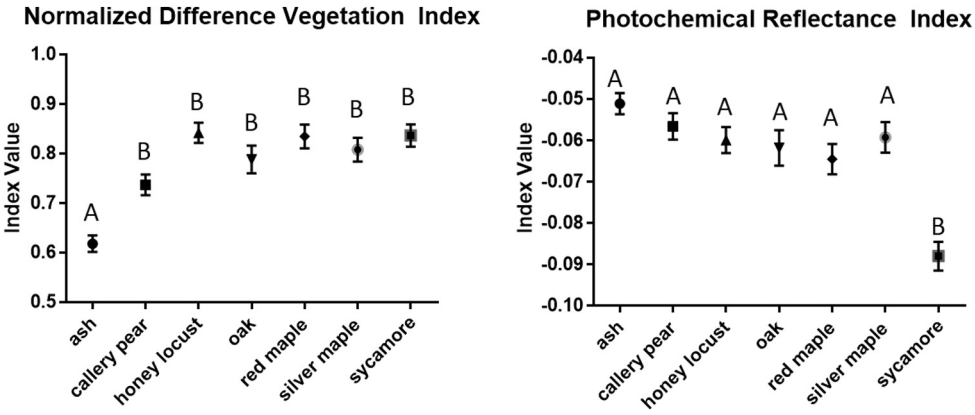

Fig. 5. An example of how various vegetation indices can help distinguish tree species regardless of canopy vigor (significance at $p < 0.0001$ denoted by A vs. B). (A) Ash species had significantly lower NDVI values compared to all other common species ($p < 0.0001$). (B) The Photochemical Reflectance Index for ash was significantly higher than sycamore but not different from all other species.

endmembers.

Many studies have used multiple endmembers to capture a range of expected spectra contained within mixed pixels (e.g. Roberts et al., 1998; Franke et al., 2009). This work demonstrates that even when considering the same target species, a range of independent spectral endmembers are required when the target is known to vary widely. This is especially important given the traditional approach of using spectral libraries or field based reflectance of "pure" spectra to classify vegetation. Given the range of ash health in the study area and the vast difference in spectra between healthy vs. stressed trees, it follows that ash species mapping efforts aimed at detecting a range of health conditions must include calibration spectra from both healthy and stressed trees as individual endmembers.

3.3. Ash classification

Our results indicate that significantly higher accuracy is achieved when utilizing hyperspectral reflectance combined with vegetation indices, and unique endmember calibration to capture the full range of ash condition. The resulting pixel-based ash probability map (Fig. 6A) can then be converted to canopy objects through image segmentation (Fig. 6B).

Based on the independent validation using the Bowie street tree inventory, overall accuracy for the 290 independent validation points resulted in 81% overall accuracy in distinguishing ash from non-ash polygons (Table 4). While overall accuracy is an improvement over other ash mapping efforts in infested regions (Murfitt et al., 2016 – 63% overall accuracy), an examination of where errors occur can better inform how the resulting mapping products can be used. Errors of commission (6%), primarily involved oak species and red maple incorrectly classified as ash (13% and 9% error of commission respectively) (Table 4). Confusion among these species may be due in part to spectral similarity as well as common association of *Fraxinus* and *Acer* species in eastern forests. Ash tends to grow tall, straight and free of branches for most of its length (Society of American Foresters Type 20). Thus, a relatively large ash tree may nevertheless be dominated by only a small apical crown, and common associates with broader crowns—such as *Acer* spp., which may be sub-canopy or co-dominant in the canopy—may confound a spectral signature within a pixel.

More significant were errors of omission (65%), suggesting that even with the unique vigor endmembers most ash canopies were missed. At the time of this study, the majority of the city's ash trees were listed in various stages of EAB induced decline. Considering that ash have relatively sparse canopies when healthy, that then become even more transparent as decline condition worsens, it is perhaps not surprising that such a large proportion of ash were missed. To verify if ash condition was contributing to high errors of omission, we compared ash identification accuracy across vigor classes on 37 calibration trees where vigor metrics were available (Table 5). Ash identification accuracy decreased from 62% for vigor 1 canopies to 22% for vigor 2 canopies. By vigor 4 none of the ash canopies included in the validation set were identified as ash. It is likely that ash in poor health contained a substantial proportion of understory or ground spectral characteristics that masked the signal of the ash canopy, confounding classification. This highlights the importance of mapping the ash resource prior to the onset of acute stressors such as EAB. Once decline reaches vigor 2 (e.g. dieback > 25%) it becomes much more difficult to identify ash canopies.

Additional error likely resulted from the translation from the 1 m resolution MTMF raster to object based canopy means used for final map creation and validation. While 1 m spatial resolution imagery allows for more precise identification of tree locations and individual crowns than would be possible with larger pixels, high spatial resolution images inherently include clusters of pixels that represent different constituents (e.g., foliage, soil, bark/woody material, understory ground cover, etc.). When aggregated as image objects, vegetation signatures can be muted by mixed pixels also grouped in that object. Thus, conversion of high resolution imagery to objects can potentially confound interpretation of the accuracy of the pixel-based spectral unmixing outputs. Considering that a portion of any crown contains a mixture of ash foliage, foliage from nearby trees, as well as bark, understory and/or other materials, it may be possible to improve ash mapping accuracy by reducing the mean probability threshold that must be met for each image object. However, we caution against arbitrarily adjusting classification thresholds to maximize classification accuracy. This makes resulting maps highly dependent on the specific validation data set used to assess various thresholds.

Over the entire study area, approximately 5% of all forest canopy objects were classified as ash. Knowing that we have probably omitted many ash trees in more advanced stages of decline, true ash cover is likely higher. In the complete Bowie street tree inventory, ash represents just over 5% of all trees. Because, the concentration of predicted ash canopies across the landscape are predominantly within the contiguous forest areas not captured in street tree inventories (Fig. 7) we believe that our results remain in line with street tree inventory in spite of our errors of omission. The location of ash in these unsurveyed areas, as well as identification of ash trees in decline is essential to manage the spread of EAB in newly infested locations.

4. Conclusions

Mapping ash species in urban environments represents an ambitious undertaking given the small size and sparse nature of ash canopies, as well as variation in abundance and condition. Even crowns from the healthiest ash trees can appear sparse given the species' propensity for apical dominance and leggy branch distribution, allowing understory targets to confound reflectance characteristics. In regions of widespread decline, "typical" canopy reflectance signatures are further

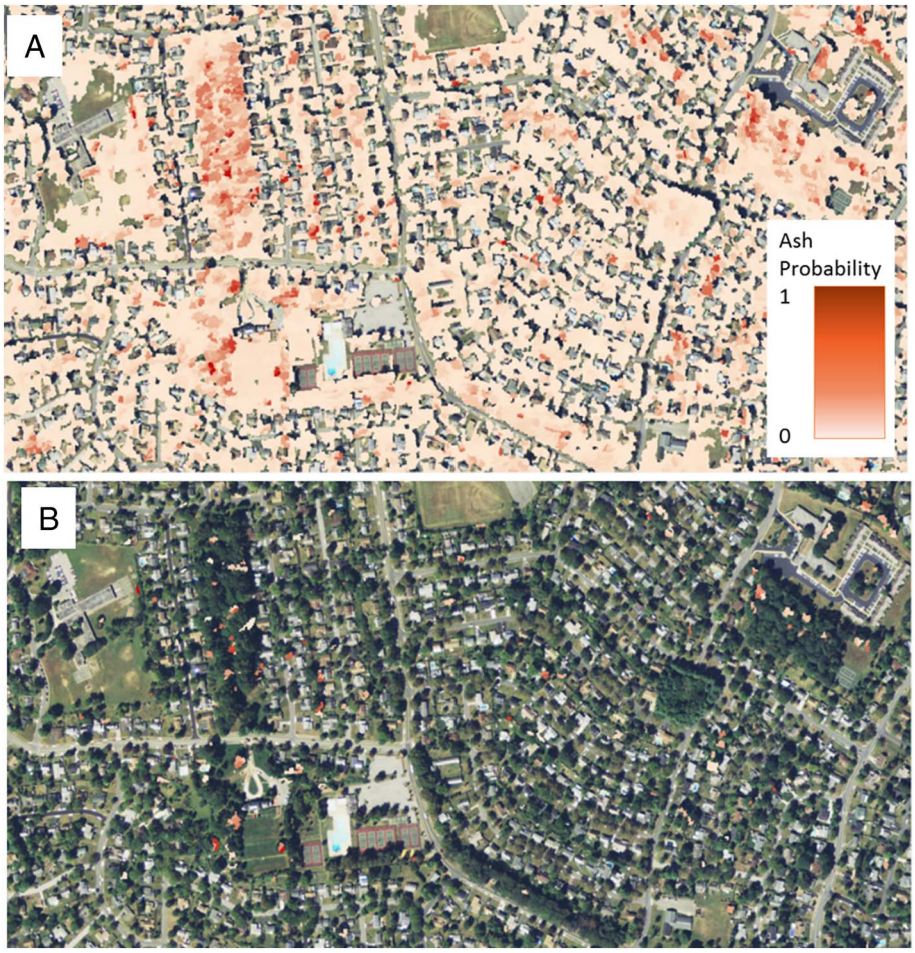

Fig. 6. A. The logistic regression calculates the probability of ash occurrence for each pixel, which is then averaged for each image object from the segmentation algorithm. B. All objects with > 0.50 probability of ash are classified as ash canopies.

compromised by changes in foliar density, chemistry and water content. Nevertheless, this study provides evidence that ash canopies can be detected with high spatial resolution, hyperspectral remote sensing imagery across a range of canopy conditions when calibration endmembers, from a range of canopy conditions, are included in classification algorithms. This approach involves high spatial resolution, hyperspectral imagery, including vegetation indices and MTMF-based spectral unmixing of ash components for each distinct ash vigor class.

While overall independent classification accuracy was good at 81%, errors of omission were particularly high, indicating that land managers must be aware that many ash are likely to be missed. Because ash classification accuracy consistently decreased with decreasing ash canopy condition, it is likely that these errors of omission are primarily missing trees in the later stages of EAB induced decline. This is likely due to changing foliar chemistry (reductions in photosynthetic structures and decrease in leaf turgor) and canopy structure. As the canopy thins, reflectance from understory herbaceous, woody stem and soil components can saturate reflectance properties (e.g., Schmidtlein, 2005), making the link to endmember ash spectra less likely. This demonstrates that spectral characteristics across a range of ash condition vary so considerably that even when classification algorithms are trained on canopies representing a range of ash conditions many declining trees are likely to be missed.

These results suggest that managing the ash resource in currently un-infested regions would benefit from the development of baseline species maps of the host species prior to infestation when canopies are relatively healthy. This baseline data can guide logistical planning and

Table 5
Ash mapping accuracy by vigor class.

	Vigor 1	Vigor 2	Vigor 3	Vigor 4
Ash	8	2	2	0
Other	5	7	5	8
Accuracy	62%	22%	29%	0%

Table 4
Accuracy across the 290 independent validation points representing the most common species and land use types in the study area.

		Actual classification								
		Ash sp.	honey locust	Oak sp.	Red maple	Silver maple	Sycamore	Callery pear	Field	Imperv. surface
Predicted classification	Ash	34	1	7	2	1	0	1	0	0
	Other	42	26	48	20	22	29	25	18	14

Ash producer's accuracy 45%
Ash user's accuracy 94%
Overall mapping accuracy 81%

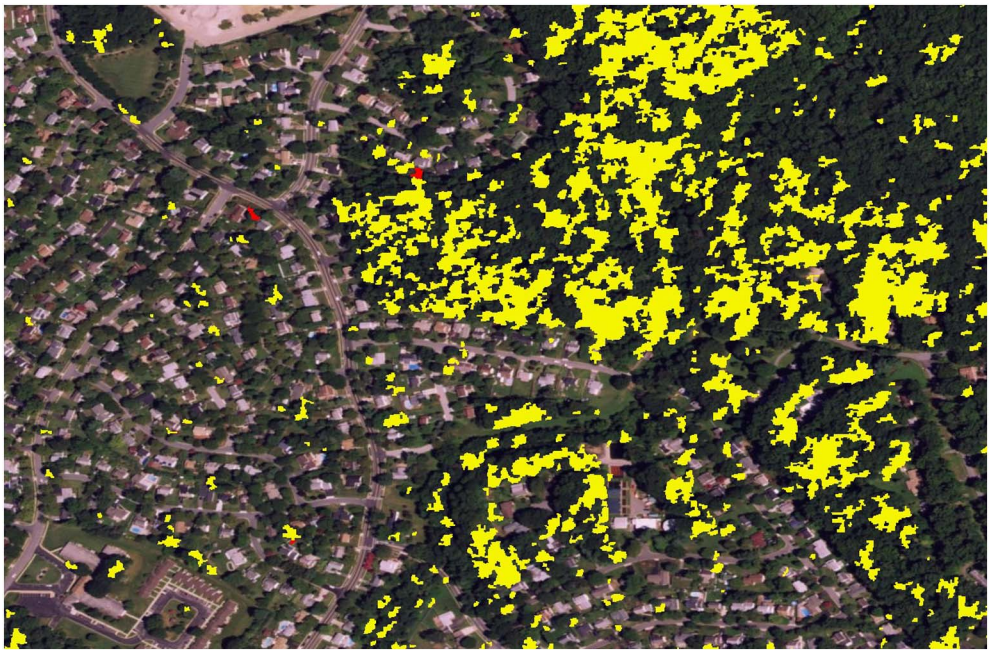

Fig. 7. Ash canopies (yellow) demonstrate the location of ash street trees, juxtaposed with the much higher ash density commonly found in larger forest tracts across the study area. (For interpretation of the references to color in this figure legend, the reader is referred to the web version of this article.)

avoid classification errors that will likely arise once infestation is well established. Subsequent remote sensing data acquisitions can take advantage of this baseline data set (known location of healthy trees) and the proven methods of mapping forest health (e.g. Pontius et al., 2005a, b, 2008) to more efficiently create updated maps of canopy condition. This approach could provide important information to guide city foresters and planners as they face infestation and subsequent decline for an important urban tree species.

Acknowledgements

The authors gratefully acknowledge the U.S. Forest Service Forest Health Technology Enterprise Team, the U.S. Forest Service Northern Research Station and the Northeastern Area State and Private Forestry Science Technology and Development Program for support. We give special thanks to the town of Bowie Maryland, who provided the field validation data that made this project possible. We are also appreciative of Noah Ahles and technicians at the University of Vermont Spatial Analysis Laboratory for assistance with image processing.

References

Aoki, M., Yabuki, K., Totsuka, T., 1981. An evaluation of chlorophyll content of leaves based on the spectral reflectivity in several plants. In: Research Report of the National Institute of Environmental Studies of Japan. 66. pp. 125–130.

Aukema, J.E., Leung, B., Kovacs, K., Chivers, C., Britton, K.O., Englin, J., Frankel, S.J., Haight, R.G., Holmes, T.P., Liebhold, A.M., McCullough, D.G., Von Holle, B., 2011. Economic impacts of non-native forest insects in the continental United States. PLoS One 6, e24587.

Baret, F., Jacquemoud, S., Guyot, G., Leprieur, C., 1992. Modeled analysis of the biophysical nature of spectral shifts and comparison with information-content of broad bands. Remote Sens. Environ. 41, 133–142.

Barnes, J.D., 1992. A reappraisal of the use of DMSO for the extraction and determination of chlorophylls a and b in lichens and higher plants. Environ. Exp. Bot. 2, 85–100.

Bauer, L.R., Haack, R.A., Miller, D.R., Petrice, T.R., Liu, H., 2004. Emerald ash borer life cycle. In: Emerald Ash Borer Research and Technology Development Meeting. Port Huron, MI.

Blackburn, G.A., 1998. Quantifying chlorophylls and caroteniods at leaf and canopy scales: an evaluation of some hyperspectral approaches. Remote Sens. Environ. 66, 273–285.

Boardman, J.W., Kruse, F.A., 2011. Analysis of imaging spectrometer data using N-dimensional geometry and a mixture-tuned matched filtering approach. IEEE Trans. Geosci. Remote Sens. 49, 4138–4152.

Broge, N.H., Leblanc, E., 2001. Comparing prediction power and stability of broadband and hyperspectral vegetation indices for estimation of green leaf area index and canopy chlorophyll density. Remote Sens. Environ. 76, 156–172.

Cappaert, D.L., McCullough, D.G., Poland, T.M., 2005. Emerald ash borer life cycle: a reassessment. In: Emerald Ash Borer Research and Technology Development Meeting. Romulus, MI.

Carter, G.A., 1994. Ratios of leaf reflectances in narrow wavebands as indicators of plant stress. Int. J. Remote Sens. 15, 697–703.

Cihlar, J., Stlaurent, L., Dyer, J.A., 1991. Relation between the normalized difference vegetation index and ecological variables. Remote Sens. Environ. 35, 279–298.

Congalton, R.G., 2001. Accuracy assessment and validation of remotely sensed and other spatial information. Int. J. Wildland Fire 10, 321–328.

Cook, B.D., Corp, L.W., Nelson, R.F., Middleton, E.M., Morton, D.C., McCorkel, J.T., Masek, J.G., Ranson, K.J., Ly, V., Montesano, P.M., 2013. NASA Goddard's Lidar, hyperspectral and thermal (G-LiHT) airborne imager. Remote Sens. Environ. 5, 4045–4066.

Cooke, R., Pendrel, B., Barnett, C., Allen, D., 1996. North American Maple Project Cooperative Field Manual. USDA Forest Service, Northeastern Area, State and Private Forestry, Durham (NH).

Datt, B., 1998. Remote sensing of chlorophyll *a*, chlorophyll *b*, chlorophyll *a* + *b*, and total carotenoid content in eucalyptus leaves. Remote Sens. Environ. 66, 111–121.

Datt, B., 1999. Visible/near infrared reflectance and chlorophyll content in eucalyptus leaves. Int. J. Remote Sens. 20, 2741–2759.

Daughtry, C.S.T., Walthall, C.L., Kim, M.S., de Colstoun, E.B., McMurtrey, J.E., 2000. Estimating corn leaf chlorophyll concentration from leaf and canopy reflectance. Remote Sens. Environ. 74, 229–239.

Dymond, C.C., Mladenoff, D.J., Radeloff, V.C., 2002. Phenological differences in tasseled cap indices improve deciduous forest classification. Remote Sens. Environ. 80, 460–472.

Elmore, A.J., Mustard, J.F., Manning, S.J., Lobell, D.B., 2000. Quantifying vegetation change in semiarid environments: precision and accuracy of spectral mixture analysis and the normalized difference vegetation index. Remote Sens. Environ. 73, 87–102.

Elvidge, C.D., Chen, Z., 1995. Comparison of broad-band and narrow band red and near-infrared vegetation indices. Remote Sens. Environ. 54, 38–48.

Filella, I., Penuelas, J., 1994. The red edge position and shape as indicators of plant chlorophyll content, biomass, and hydric status. Int. J. Remote Sens. 15, 1459–1470.

Franke, J., Roberts, D.A., Halligan, K., Menz, G., 2009. Hierarchical multiple endmember spectral mixture analysis (MESMA) of hyperspectral imagery for urban environments. Remote Sens. Environ. 113 (8), 1712–1723.

Gamon, J.A., Surfus, J.S., 1999. Assessing leaf pigment content and activity with a reflectometer. New Phytol. 143, 105–117.

Gamon, J.A., Field, C.B., Bilger, W., Bjorkman, O., Fredeen, A.L., Penuelas, J., 1990. Remote-sensing of the xanthophyll cycle and chlorophyll fluorescence in sunflower leaves and canopies. Oecologia 85, 1–7.

Gamon, J.A., Serrano, L., Surfus, J.S., 1997. The photochemical reflectance index: an optical indicator of photosynthetic radiation use efficiency across species, functional types, and nutrient levels. Oecologia 112, 492–501.

Gitelson, A., Merzlyak, M.N., 1994. Spectral reflectance changes associated with autumn senescence of Aesculus hippocastanum L. and Acer platanoides L. leaves. Spectral features and relation to chlorophyll estimation. J. Plant Physiol. 143, 286–292.

Gitelson, A.A., Merzlyak, M.N., Chivkunova, O.B., 2001. Optical properties and non-destructive estimation of anthocyanin content in plant leaves. Photochem. Photobiol. 74, 38–45.

Gitelson, A.A., Gritz, U., Merzlyak, M.N., 2003. Relationships between leaf chlorophyll content and spectral reflectance and algorithms for non-destructive chlorophyll assessment in higher plant leaves. J. Plant Physiol. 160, 271–282.

Green, R.O., Eastwood, M.L., Sarture, C.M., Chrien, T.G., Aronsson, M., Chippendale, B.J., Faust, J.A., Pavri, B.E., Chovit, C.J., Solis, M.S., Olah, M.R., Williams, O., 1998. Imaging spectroscopy and the airborne visible infrared imaging spectrometer (AVIRIS). Remote Sens. Environ. 65, 227–248.
Haack, R.A., Jendak, E., Houping, L., Marchant, K.R., Petrice, T.R., Poland, T.M., Ye, H., 2002. The emerald ash borer: a new exotic pest in North America. In: Newsletter of the Michigan Entomological Society. 47. pp. 1–5.
Haboudane, D., Miller, J.R., Pattey, E., Zarco-Tejada, P.J., Strachan, I.B., 2004. Hyperspectral vegetation indices and novel algorithms for predicting green LAI of crop canopies: modeling and validation in the context of precision agriculture. Remote Sens. Environ. 90, 337–352.
Homer, C., Dewitz, J., Yang, L., Jin, S., Danielson, P., Xian, G., Coulston, J., Herold, N., Wickham, J., Megown, K., 2015. Completion of the 2011 National Land Cover Database for the conterminous United States - representing a decade of land cover change information. Photogramm. Eng. Remote. Sens. 81, 345–354.
Kerr, J., Ostrovsky, M., 2003. From space to species: ecological applications for remote sensing. Trends Ecol. Evol. 18, 299–305.
Keshava, N., Mustard, J.F., 2002. Spectral unmixing. IEEE Signal Process. Mag. 19 (1), 44–57.
Klooster, W., Herms, D., Knight, K., Herms, C., McCullough, D., Smith, A., Gandhi, K.K., Cardina, J., 2014. Ash (Fraxinus spp.) mortality, regeneration, and seed bank dynamics in mixed hardwood forests following invasion by emerald ash borer (Agrilus planipennis). Biol. Invasions 16, 859–873.
Kovacs, K.F., Haight, R.G., McCullough, D.G., Mercader, R.J., Siegert, N.W., Liebold, A.M., 2010. Cost of potential emerald ash borer damage in US communities: 2009–2019. Ecol. Econ. 69, 569–578.
Liebhold, A.M., MacDonal, W.L., Bergdahl, D., Mastro, V.C., 1995. Invasion by exotic forest pests: a threat to forest ecosystems. For. Sci. 41, 1–49.
Maccioni, A., Agati, G., Mazzinghi, P., 2001. New vegetation indices for remote measurement of chlorophylls based on leaf directional reflectance spectra. J. Photochem. Photobiol. 61, 52–61.
Martin, M.E., Newman, S.D., Aber, J.D., Congalton, R.G., 1998. Determining forest species composition using high spectral resolution remote sensing data. Remote Sens. Environ. 65, 249–254.
McCullough, D.G., Poland, T.M., Anulewicz, A.C., Cappaert, D., 2009. Emerald ash borer (Coleoptera: Buprestidae) attraction to stressed or baited ash trees. Environ. Entomol. 38, 1668–1679.
de Melo Figueiredo, S.M., Venticinque, E.M., Figueiredo, E.O., Linhares Ferreira, E.J., 2015. Predicting the distribution of forest tree species using topographic variables and vegetation index in eastern acre, Brazil. Acta Amazon. 45, 167–174.
Merzlyak, M.N., Gitelson, A.A., Chivkunova, O.B., Rakitin, V.Y., 1999. Non-destructive optical detection of pigment changes during leaf senescence and fruit ripening. Physiol. Plant. 106, 135–141.
Miao, X., Gong, P., Swope, S., Pu, R.L., Carruthers, R., Anderson, G.L., Heaton, J.S., Tracy, C.R., 2006. Estimation of yellow starthistle abundance through CASI-2 hyperspectral imagery using linear spectral mixture models. Remote Sens. Environ. 101, 329–341.
Mohammed, G.H., Binder, W.D., Gillies, S.L., 1995. Chlorophyll fluorescence - a review of its practical forestry applications and instrumentation. Scand. J. For. Res. 10, 383–410.
Murfitt, J., He, Y.H., Yang, J., Mui, A., De Mille, K., 2016. Ash decline assessment in emerald ash borer infested natural forests using high spatial resolution images. Remote Sens. 8.
Niemelä, P., Mattson, W.J., 1996. Invasion of North American forests by European phytophagous insects. Bioscience 46, 741–753.
Pearson, L., Miller, L.D., 1972. Remote mapping of standing crop biomass for estimation of the productivity of the short-grass prairie, Pawnee National Grasslands, Colorado. In: Proceedings of the 8th International Symposium on Remote Sensing of the Environment. ERIM, Ann Arbor, MI, pp. 1357–1381.
Peddle, D.R., Brunke, S.P., Hall, F.G., 2001. A comparison of spectral mixture analysis and ten vegetation indices for estimating boreal forest biophysical information from airborne data. Can. J. Remote. Sens. 27, 627–635.
Penuelas, J., Filella, I., Biel, C., Serrano, L., Save, R., 1993. The reflectance at the 950–970 nm region as an indicator of plant water status. Int. J. Remote Sens. 14, 1887–1905.
Penuelas, J., Gamon, J.A., Fredeen, A.L., Merino, J., Field, C.B., 1994. Reflectance indices associated with physiological changes in nitrogen-limited and water-limited sunflower leaves. Remote Sens. Environ. 48, 135–146.
Penuelas, J., Baret, F., Filella, I., 1995. Semi-empirical indices to assess carotenoids/chlorophyll a ratio from leaf spectral reflectance. Photosynthetica 31, 221–230.
Pimentel, D., McNair, S., Janecka, J., Wightman, J., Simmonds, C., O'Connell, C., Wong, E., Russel, L., Zern, J., Aquino, T., Tsomondo, T., 2001. Economic and environmental threats of alien plant, animal, and microbe invasions. Agric. Ecosyst. Environ. 84, 1–20.
Plaza, A., Benediktsson, J.A., Boardman, J.W., Brazile, J., Bruzzone, L., Camps-Valls, G., Chanussot, J., Fauvel, M., Gamba, P., Gualtieri, A., Marconcini, M., Tilton, J.C., Trianni, G., 2009. Recent advances in techniques for hyperspectral image processing. Remote Sens. Environ. 113, S110–S122.
Plourde, L.C., Ollinger, S.V., Smith, M.-L., Martin, M.E., 2007. Estimating species abundance in a northern temperate forest using spectral mixture analysis. Photogramm. Eng. Remote. Sens. 73, 829–840.
Pontius, J., 2014. A new approach for forest decline assessments: maximizing detail and accuracy with multispectral imagery. Int. J. Remote Sens. 35, 3384–3402.
Pontius, J., Hallett, R., 2014. Comprehensive methods for earlier detection and monitoring of forest decline. For. Sci. 60.6, 1156–1163.
Pontius, J., Hallett, R., Martin, M., 2005a. Assessing hemlock decline using visible and near-infrared spectroscopy: indices comparison and algorithm development. Appl. Spectrosc. 59, 836–843.
Pontius, J., Hallett, R., Martin, M., 2005b. Using AVIRIS to assess hemlock abundance and early decline in the Catskills, New York. Remote Sens. Environ. 97, 163–173.
Pontius, J., Martin, M., Plourde, L., Hallett, R., 2008. Ash decline assessment in emerald ash borer-infested regions: a test of tree-level, hyperspectral technologies. Remote Sens. Environ. 112, 2665–2676.
Rahman, A.F., Gamon, J.A., Fuentes, D.A., Roberts, D.A., Prentiss, D., 2001. Modeling spatially distributed ecosystem flux of boreal forest using hyperspectral indices from AVIRIS imagery. J. Geophys. Res.-Atmos. 106, 33579–33591.
Roberts, D.A., Gardner, M., Church, R., Ustin, S., Scheer, G., Green, R.O., 1998. Mapping chaparral in the Santa Monica Mountains using multiple endmember spectral mixture models. Remote Sens. Environ. 65 (3), 267–279.
Rondeaux, G., Steven, M., Baret, F., 1996. Optimization of soil-adjusted vegetation indices. Remote Sens. Environ. 55, 95–107.
Roujean, J.-L., Breon, F.-M., 1995. Estimating PAR absorbed by vegetation from bidirectional reflectance measurements. Remote Sens. Environ. 51, 375–384.
Rouse, J.W., Haas, R.S., Schell, J.A., Deering, D.W., 1973. Monitoring vegetation systems in the Great Plains with ERTS. In: Proceedings, 3rd ERT S Symposium. 1. pp. 48–62.
Schmidtlein, S., 2005. Imaging spectroscopy as a tool for mapping Ellenberg indicator values. J. Appl. Ecol. 42, 966–974.
Simberloff, D., 2000. Nonindigenous species: a global threat to biodiversity and stability. In: Raven, P., W. T. (Eds.), Nature and Human Society: The Quest for a Sustainable World. National Academy Press, Washington, DC, pp. 325–336.
Sims, D.A., Gamon, J.A., 2002. Relationships between leaf pigment content and spectral reflectance across a wide range of species, leaf structures and developmental stages. Remote Sens. Environ. 81, 337–354.
Small, C., 2001. Estimation of urban vegetation abundance by spectral mixture analysis. Int. J. Remote Sens. 22, 1305–1334.
Smith, R.C.G., Adams, J., Stephens, D.J., Hick, P.T., 1995. Forecasting wheat yield in a Mediterranean-type environment from the NOAA satellite. Aust. J. Agric. Res. 46, 113–125.
Souci, J.S., Hanou, I., Puchalski, D., 2009. High-resolution remote sensing image analysis for early detection and response planning for emerald ash borer. Photogramm. Eng. Remote. Sens. 75, 905–909.
Sydnor, T.D., Bumgardner, M., Todd, A., 2007. The potential economic impacts of emerald ash borer (*Agrilus planipennis*) on Ohio, U.S., communities. Arboricult. Urban For. 33, 48–54.
Tucker, C.J., 1979. Red and photographic infrared linear combinations for monitoring vegetation. Remote Sens. Environ. 8, 127–150.
Ustin, S.L., Xiao, Q.F., 2001. Mapping successional boreal forests in interior central Alaska. Int. J. Remote Sens. 22, 1779–1797.
Vogelmann, J.E., Rock, B.N., Moss, D.M., 1993. Red edge spectral measurements from sugar maple leaves. Int. J. Remote Sens. 14, 1563–1575.
Waring, R.H., Coops, N.C., Fan, W., Nightingale, J.M., 2006a. MODIS enhanced vegetation index predicts tree species richness across forested ecoregions in the contiguous U.S.A. Remote Sens. Environ. 103, 218–226.
Waring, R.H., Coops, N.C., Fan, W., Nightingale, J.M., 2006b. MODIS enhanced vegetation index predicts tree species richness across forested ecoregions in the contiguous USA. Remote Sens. Environ. 103, 218–226.
Williams, A.P., Hunt, E.R., 2002. Estimation of leafy spurge cover from hyperspectral imagery using mixture tuned matched filtering. Remote Sens. Environ. 82, 446–456.
Yang, J., He, Y., Caspersen, J., 2014a. A multi-band watershed segmentation method for individual tree crown delineation from high resolution multispectral aerial image. In: IGARSS 2014. IEEE: EI, Quebec, Canada, pp. 1588–1591.
Yang, J., Li, P., He, Y., 2014b. A multi-band approach to unsupervised scale parameter selection for multi-scale image segmentation. ISPRS J. Photogramm. Remote Sens. 94, 13–24. http://dx.doi.org/10.1016/j.isprsjprs.2014.04.008.
Yang, J., He, Y., Caspersen, J., Jones, T., 2015. A discrepancy measure for segmentation evaluation from the perspective of object recognition. ISPRS J. Photogramm. Remote Sens. 101, 186–192. http://dx.doi.org/10.1016/j.isprsjprs.2014.12.015.
Zarco-Tejada, P.J., Miller, J.R., Mohammed, G.H., Noland, T.L., Sampson, P.H., 2002. Vegetation stress detection through chlorophyll $_{a+b}$ estimation and fluorescence effects on hyperspectral imagery. J. Environ. Qual. 31, 1433–1441.
Zhang, Kongwen, Hu, Baoxin, Robinson, Justin, 2014. Early detection of emerald ash borer infestation using multisourced data: a case study in the town of Oakville, Ontario, Canada. J. Appl. Remote. Sens. 8 (1) (083602-083602).